Quantum Semiclass. Opt. **10** (1998) 239–250. Printed in the UK PII: S1355-5111(98)85473-0

Experimental method to detect the magnetic birefringence of vacuum

D Bakalov[a]†, F Brandi[a b], G Cantatore[c], G Carugno[d], S Carusotto[b e], F Della Valle[c], A M De Riva[f], U Gastaldi[a], E Iacopini[g], P Micossi[c], E Milotti[c], R Onofrio[d h], R Pengo[a], F Perrone[b e], G Petrucci[a], E Polacco[b e], C Rizzo[a]‡, G Ruoso[d h], E Zavattini[c] and G Zavattini[f]

[a] Laboratori INFN, via Romea 4, 35020 Legnaro (PD), Italy
[b] Dipartimento di Fisica, Piazza Torricelli 1, 56100 Pisa, Italy
[c] Dipartimento di Fisica and INFN, via Valerio 2, 34127 Trieste, Italy
[d] INFN, Sezione di Padova, via Marzolo 8, 35131 Padova, Italy
[e] INFN, Sezione di Pisa, via Livornese 582/a, 56010 S Piero a Grado (PI), Italy
[f] Dipartimento di Fisica and INFN, via Paradiso 12, 44100 Ferrara, Italy
[g] Dipartimento di Fisica and INFN, largo E Fermi 2, 50125 Firenze, Italy
[h] Dipartimento di Fisica 'Galileo Galilei', via Marzolo 8, 35131 Padova, Italy

Received 13 June 1997, in final form 30 September 1997

Abstract. We describe the principle and the status of the PVLAS experiment which is being assembled at INFN Laboratori Nazionali di Legnaro (Legnaro, Padua, Italy) to look for coherent effects, related to the QED vacuum structure, on the propagation of a polarized light beam in a strong magnetic field.

1. Introduction

Maxwell's electromagnetic theory, modified to be consistent with quantum principles, has given rise to quantum electrodynamics (QED). Among the novel phenomena described by QED and as yet never observed experimentally one has to include the so-called vacuum magnetic birefringence [1]. Vacuum, under the influence of a magnetic field, should show a different refractive index for light polarized parallel or orthogonal to the magnetic field direction.

The purpose of the PVLAS [2] (Polarizzazione del Vuoto con Laser) experiment is to measure for the first time this small anisotropy caused by the presence of the static field $\boldsymbol{B}_0$ perpendicular to the direction of the propagating beam. The experimental method adopted is the one suggested in [3].

Below we present the formulae necessary to understand the measurements to be performed. Then we describe the status of the PVLAS experiment which is being assembled at Legnaro INFN National Laboratories (LNL). Finally, we mention briefly some possible hypothetical processes, not specifically within QED, which might contribute to the detectable optical activity of the vacuum.

† On leave from: Institute for Nuclear Research and Nuclear Energy, tsarigradsko chaussee 72, Sofia 1784, Bulgaria.

‡ On leave from: INFN, Sezione di Trieste, via Valerio 2, 34127 Trieste, Italy. Author to whom correspondence should be addressed.

1355-5111/98/010239+12$19.50

2. Introductory formulae

It has been shown in quantum electrodynamics [4–7] that the propagation of an electromagnetic wave in an empty region, where a quasi-constant magnetic field is present, can be described by Maxwell's equations supplemented by constitutive relations. These relations, linking the vector fields $\boldsymbol{D}$ and $\boldsymbol{H}$ with the vector fields $\boldsymbol{E}$ and $\boldsymbol{B}$, are deduced from the appropriate effective Lagrangian L_{e} provided by quantum electrodynamics.

We therefore write (in Gaussian units):

$$\begin{aligned} &\nabla \times \boldsymbol{E} = -\frac{1}{c}\frac{\partial \boldsymbol{B}}{\partial t} \qquad \nabla \cdot \boldsymbol{B} = 0 \\ &\nabla \times \boldsymbol{H} = \frac{1}{c}\frac{\partial \boldsymbol{D}}{\partial t} \qquad \nabla \cdot \boldsymbol{D} = 0 \end{aligned} \tag{1}$$

$$D_i = 4\pi \frac{\partial L_{\mathrm{e}}}{\partial E_i} \qquad H_i = -4\pi \frac{\partial L_{\mathrm{e}}}{\partial B_i} \qquad i = 1, 2, 3$$

$$L_{\mathrm{e}} = (1/4\pi)[F + 4aA_{\mathrm{e}}F^2 + 7bA_{\mathrm{e}}G^2] \tag{2}$$

where

$$F = \frac{E^2 - B^2}{2} \qquad G = \boldsymbol{E} \cdot \boldsymbol{B} \qquad a = 1 + \sqrt{2}\alpha \qquad b = 1 + \tfrac{5}{3}\alpha$$

and

$$A_{\mathrm{e}} = \frac{\alpha^2(\lambda_{\mathrm{e}}/2\pi)^3}{90\pi mc^2} = \tfrac{4}{3} \times 10^{-32}\ \mathrm{cm}^3\ \mathrm{erg}^{-1}$$

with α the fine structure constant, λ_{e} the electron Compton wavelength, m the electron rest mass, and $\boldsymbol{B}$ and $\boldsymbol{E}$ the magnetic and electric fields, respectively. The first term in (2) is equal to the classical Maxwellian Lagrangian; in this approximation, all QED radiative corrections are represented by the terms proportional to A_{e}.

We will see that, for our set-up, the coefficients $4aA_{\mathrm{e}}$ and $7bA_{\mathrm{e}}$ in expression (2) assume a specific physical interpretation. Notice that, owing to the vacuum positron–electron virtual currents, there appear terms describing an indirect photon–photon (or better photon–external field) interaction responsible for the nonlinearity.

Let us recall that the approximate expression (2) for L_{e} is assumed to be valid under some general conditions [4]; here it is enough to write: (i) $B \ll 4.4 \times 10^{13}$ G; (ii) terms with α to the fourth or higher powers are not considered; (iii) terms containing contributions of virtual charged particle–antiparticle pairs other than those from the positron–electron quantum field are excluded.

Let us now study the propagation of laser radiation, with an associated field $B(t)$, in an external transverse magnetic field $B_0 \gg B(t)$.

The total field $\boldsymbol{B}$ can be written as

$$\boldsymbol{B} = \boldsymbol{B}_0 + \boldsymbol{B}(t).$$

In deriving the constitutive relations we will retain only linear terms in fields $\boldsymbol{B}(t)$ and $\boldsymbol{E}(t)$. With these assumptions and (1) and (2) one obtains

$$\begin{aligned} \boldsymbol{D}(t) &= \boldsymbol{E}(t)\big[1 - 4aA_{\mathrm{e}}B_0^2\big] + 14bA_{\mathrm{e}}\boldsymbol{B}_0(\boldsymbol{B}_0 \cdot \boldsymbol{E}(t)) \\ \boldsymbol{H}(t) &= \boldsymbol{B}(t)\big[1 - 4aA_{\mathrm{e}}B_0^2\big] - 8aA_{\mathrm{e}}\boldsymbol{B}_0(\boldsymbol{B}_0 \cdot \boldsymbol{B}(t)). \end{aligned} \tag{3}$$

Considering the case in which the electric field $\boldsymbol{E}(t)$ is perpendicular to the field $\boldsymbol{B}_0$, we have for the electric permittivity and magnetic permeability of the vacuum and for the

corresponding refractive index

$$\begin{aligned}\varepsilon_\perp &= 1 - 4aA_eB_0^2\\ \mu_\perp &= 1 + 12aA_eB_0^2\\ (n_\perp - 1) &= 4aA_eB_0^2.\end{aligned} \tag{4}$$

Alternatively, in the case where the electric field $\boldsymbol{E}(t)$ is parallel to $\boldsymbol{B}_0$, one has

$$\begin{aligned}\varepsilon_\parallel &= 1 + (14b - 4a)A_eB_0^2\\ \mu_\parallel &= 1 + 4aA_eB_0^2\\ (n_\parallel - 1) &= 7bA_eB_0^2.\end{aligned} \tag{5}$$

From expressions (4) and (5) we see that for the radiation beam the empty region where $B_0 \neq 0$ appears as a weak uniaxial crystal, i.e. it shows a birefringence. Notice that the expressions for $n_\perp - 1$ and $n_\parallel - 1$ (both > 0) are determined, respectively, apart from a common B_0^2 factor, by the coefficient of F^2, $4aA_e$, and the coefficient of G^2, $7bA_e$, in expression (2).

In conclusion, from expressions (4) and (5) one obtains

$$\Delta n = 4 \times 10^{-32}(1 + 0.015)B_0^2 \tag{6}$$

where B_0 is measured in Gauss. The small correction of 1.5% comes from the radiative corrections to the leading α^2 term.

The task of the PVLAS experiment is to detect and measure the small anisotropy indicated by equation (6).

3. Detection technique

In the presence of the magnetically induced anisotropy in the refractive index, the birefringence shown by the vacuum after the light has propagated along an optical path L is

$$\delta = 2\pi \frac{L}{\lambda}\Delta n \sin(2\theta) \tag{7}$$

where θ is the angle between the light polarization and the direction of the transverse magnetic field and λ is the wavelength of the light.

In the case of a very small birefringence, the initially linearly polarized light beam acquires, during propagation in the birefringent medium, an ellipticity Ψ related to the birefringence by the formula [8]

$$\Psi = \frac{\delta}{2} = \pi \frac{L}{\lambda}\Delta n \sin(2\theta). \tag{8}$$

In the PVLAS experiment the heterodyne detection technique will be used, this technique is described using figure 1. A laser beam is linearly polarized by a polarizer prism P. The angle between the field $\boldsymbol{B}_0$ and the radiation field $\boldsymbol{E}$ is θ. Passing through the magnetic field region the light acquires an ellipticity $\Psi(t)$. Let us assume that $\Psi(t)$ can be written as $\Psi(t) = \Psi_0 \cos(2\pi\Omega t + \theta_\Psi)$. The radiation then goes through the ellipticity modulator, an optical device that gives to the beam an ellipticity φ ($\gg \Psi$), so that we can assume that $\varphi(t) = \varphi_0 \cos(2\pi\omega t + \theta\varphi)$. The polarization of the beam is finally analysed by a polarizer prism A crossed at the maximum extinction σ^2 with the polarizer prism P.

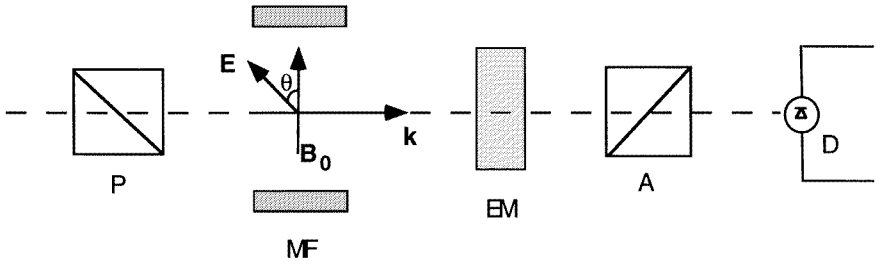

Figure 1. Scheme of an experimental set-up designed for the heterodyne technique: P, polarizer prism; MF, magnetic field region; EM, ellipticity modulator; A, analyser prism; D, photodiode.

Any optical element also acts as a birefringent medium. To take this effect into account we introduce the static ellipticity Γ. The light intensity I seen by the photodiode D can be written as

$$I = I_0\left[\sigma^2 + (\Psi + \varphi + \Gamma)^2\right] \tag{9}$$

where I_0 is the light intensity before the analyser A. The photodiode converts the intensity I into a current signal, with a power spectrum which can be studied via Fourier transform techniques. In table 1 we list the amplitudes and phases of the relevant spectral components of the signal as indicated by equation (9). The ellipticity Ψ_0 can be extracted from the formula

$$\frac{\Psi_0}{\varphi_0} = \frac{I_+}{2I_\omega} = \frac{I_-}{2I_\omega} \tag{10}$$

and the phase of the effect is given by

$$\theta_\varphi = \frac{(\theta_+ - \theta_-)}{2} \tag{11}$$

where $I_+, I_-, \theta_+, \theta_-$ are defined in table 1.

Table 1. Relevant spectral components of the signal as given in equation (9).

Frequency	Fourier component	Amplitude	Phase
0	DC	$\sigma^2 + \varphi_0^2/2$	
ω	I_ω	$2\Gamma\varphi_0$	θ_φ
$\Omega \pm \omega$	$I_\pm$	$\Psi_0\varphi_0$	$\theta_\pm = \theta_\varphi \pm \theta_\Psi$
2ω	$I_{2\omega}$	$\varphi_0^2/2$	$2\theta_\varphi$

The limiting noise level comes from the quantum noise due to the corpuscular nature of light (shot noise) [10]. The shot noise due to the Poisson distribution of the photon counting is proportional to the square root of the number of photons seen by the photodiode D per second, that is

$$i_{\text{shot noise}} \propto \sqrt{\frac{2e^2 I_0(\sigma^2 + \Gamma^2 + \varphi_0^2/2)q}{h\nu}} \tag{12}$$

where ν is the frequency of the light, q is the quantum efficiency of the photodiode, e is the electron charge and h is Planck's constant. The rate of photons corresponding to the signal seen by the photodiode D is proportional to $I_\pm$:

$$i_{\text{signal}} \propto \frac{eI_\pm q}{h\nu} = \frac{eI_0\Psi_0\varphi_0 q}{h\nu}. \tag{13}$$

The signal-to-noise ratio is therefore

$$\frac{i_{\text{signal}}}{i_{\text{shot noise}}} = \sqrt{\frac{I_0 \Psi_0^2 \varphi_0^2}{(2\sigma^2 + 2\Gamma^2 + \varphi_0^2)h\nu}}\, q. \tag{14}$$

Optimal working conditions thus imply that $\sigma^2 + \Gamma^2 \ll \varphi_0^2/2$. In this case, by imposing the condition of a signal-to-noise ratio equal to one, one obtains an expression for the sensitivity Ψ_{sens}:

$$\Psi_{\text{sens}} = \sqrt{\frac{h\nu}{I_0 q}} \tag{15}$$

with $I_0 = 15$ mW $= 1.5 \times 10^5$ erg s^{-1}, $q = 0.7$ and $\nu = 2.82 \times 10^{14}$ Hz ($\lambda = 1064$ nm), Ψ_{sens} can be as low as 4.3×10^{-9} rad Hz$^{-1/2}$.

4. The optical apparatus

The optical apparatus that we are currently testing is based on the principles discussed in the previous section. To increase the optical path L in the magnetic field region we use a Fabry–Perot cavity [8]. This is a resonant optical cavity formed by two interferential mirrors of reflectivity R. The use of the Fabry–Perot cavity increases the optical path by a factor of g [11]

$$g = \frac{2F}{\pi} \tag{16}$$

where $F = \pi R^{1/2}/(1 - R)$ is the so-called finesse of the Fabry–Perot cavity. To be in resonance the length of the cavity has to be an integer multiple of half the wavelength of the light. To fulfil this condition we lock the frequency [12] of the laser to the cavity using the Pound–Drever locking technique [13]. In figure 2 a simplified scheme of the optical apparatus is shown.

The light source is a tunable NPRO (non-planar ring oscillator) Nd:YAG laser emitting about 110 mW of power at a wavelength $\lambda = 1.064$ μm ($\nu = 2.82 \times 10^{14}$ Hz). The laser light after crossing a two-stage optical isolator OI, enters the polarizing cube beamsplitter P, which is set for maximum transmission. The Faraday cell FC rotates the polarization by a 45° angle and a half-wave plate $\lambda/2$ is used to change the polarization direction of the beam. A telescope TL is used to match the laser beam to the cavity FP. Mirrors M_1 and M_2 are mounted on tilting stages and are used to allow alignment of the beam with the optical axis of the cavity. When the cavity and the beam are properly aligned light coming back from the cavity follows the same optical path as incoming light. After crossing the Faraday cell FC the polarization angle of the reflected light is rotated a further 45° so that the reflected light can be extracted from the main path as the ordinary ray of polarizer prism P. Mirror M_3 steers the beam in the vertical direction. The polarizer prism PP is used to linearly polarize the laser beam before entering the FP cavity formed by the two mirrors CM_1 and CM_2. While stored in the Fabry–Perot cavity the light acquires the ellipticity to be measured due to the presence of the magnetic field given by a superconducting dipole magnet DM. The magnet in its cryostat will be seated on a rotating table RT. Thus we will change the angle θ between the polarization direction of the light and the direction of the magnetic field:

$$\theta = 2\pi \Omega_{\text{m}} t + \theta_{\text{m}}. \tag{17}$$

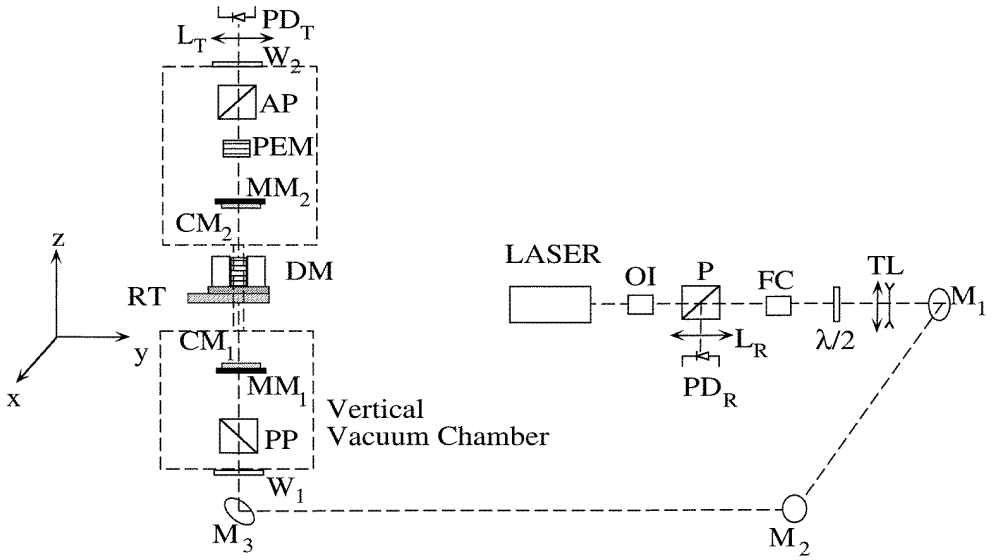

Figure 2. Simplified scheme of the apparatus. OI, optical isolator; P, PP, AP, polarizer prisms; L_R, L_T, lenses; PD_R, PD_T, photodiodes; FC, Faraday cell; $\lambda/2$, half-wave plate; TL, telescope; M_1, M_2, M_3, steering mirrors; W_1, W_2, windows; MM_1, MM_2, tilting stages; CM_1, CM_2, cavity mirrors; RT, rotating table; DM, dipole magnet; PEM, photo-elastic modulator; the coordinate axes are also shown.

Using equation (8) it is straightforward to see that the resulting ellipticity Ψ will be modulated at a frequency $\Omega = 2\Omega_m$ and that the phase $\theta_\Psi = 2\theta_m$. The light transmitted by the cavity passes through a photoelastic ellipticity modulator PEM. This device consists of a slab of fused silica on which a piezoelectric device induces a high stress birefringence longitudinally when driven by a sinusoidal wave at the mechanical resonance frequency of the longitudinal mode of the slab itself. The polarizer prism AP is then used to analyse the polarization state of the light transmitted by the cavity. The cavity mirrors CM_1 and CM_2, the polarizer prisms PP and AP and the PEM are contained in a vacuum chamber and mounted on stages designed to rotate the optical elements around the z axis, to tilt them around the x and y axes and to translate along the x and y axes (see figure 2). Appropriate manual feedthroughs for vacuum allow us to precisely align the optical elements from outside the vertical vacuum chamber. The photodiode PD_R collects the reflected light, focused by the lens L_R, giving the main signal for the Pound–Drever locking scheme. The photodiode PD_T, on the other hand, collects the light transmitted by the cavity and analysed by the polarizer prism AP. The lens L_T focuses the transmitted light onto this photodiode. Two windows W_1 and W_2 allow the light to enter and exit the vacuum chamber.

5. Magnet and cryostat [14]

In the PVLAS experiment an 8 T superconducting dipole magnet cooled by superfluid helium will be used. This magnet has been designed, realized and tested at CERN [15] within the framework of the tests following the 1979 proposal [3].

The magnet has been operated immersed in a superfluid helium bath at a temperature of 1.8 K and a pressure of 1 bar. The dipole is wound with a hollow Cu–Nb–Ti composite conductor. The conductor has a square cross section of 5.5×5.5 mm^2 with a central bore of

approximately 2.5 mm diameter. The dipole has two identical coils mounted symmetrically with respect to the medium plane. The dipole also has a soft iron yoke which has the dual purpose of slightly enhancing the magnetic field, and of providing a very rigid structure to withstand the very large electromagnetic forces. Aluminium alloy plates and bolts are used to clamp together the various parts of the yoke. When the magnet is cooled down (by reason of the larger thermal contraction of the aluminium alloy) the coils are strongly precompressed in the vertical and horizontal directions. During 1982 tests an almost complete absence of coil training was noted. This fact was attributed to the very rigid mechanical support of the coils and to the small amount of superfluid helium contained in the hollow superconductor, which greatly enhances the coil enthalpy stabilization. In table 2 we list the main parameters of the magnet.

Table 2. Main parameters of the magnet.

Cold bore useful diameter	0.1 m
Magnetic field length	1 m
Overall magnet length	1.3 m
Central field	8 T
Current (for a central field of 8 T)	3810 A
Maximum field on the conductor	8.8 T
Field uniformity in the useful bore	$\pm 2.5\%$
Average current density in the winding	105 A mm^{-2}
Stored energy	1.5 MJ

In figure 3 we show a schematic diagram of the cryostat that is currently under test at the Legnaro Laboratories. The vertical cryostat is subdivided into two parts by a thick insulating plate of glass epoxy material. The dipole is located in the bottom part. At the beginning of the operation (after preliminary precooling by means of liquid nitrogen) the cryostat is completely filled with liquid helium at 4.2 K. Pumping helium (at low pressure, about 16 Torr) through the J–T (Joule–Thomson) expansion valve, low-temperature helium is produced in the heat exchanger. By conduction the helium contained in the bottom of the cryostat, below the glass epoxy plate, can be cooled down to 1.8 K. A temperature gradient is built up in the helium contained in the cryostat above the insulating plate. The temperature is just above the λ point (2.17 K) on the upper face of the plate and rises to 4.2 K on the liquid surface. During normal operations in the bottom part of the cryostat no vapour is present, if any problem should occur an emergency cold valve allows the vapour produced to reach the upper part and be extracted. On the magnet several detectors will be used to check the coils' temperature and alert a quench protection system to avoid any damage to the magnet itself in case of quench.

The whole cryostat during data taking will rotate around its axis; during rotation the electrical connection with the outside world will be interrupted and the magnet will run in permanent current mode. A switch S, put in the 4.2 K region of the cryostat, will allow us to short circuit the magnet when properly charged. While in rotation cryogenics connection will also be interrupted, and the pump group that pumps on the heat exchanger will rotate with the cryostat. A servo system will regulate the gas flow in the two-phase heat exchanger through the adjustment of the J–T needle valve. Special care has to be taken with respect to the centring of the room temperature hole in the centre of the cryostat, where the vacuum pipe is located. The bare hole of the magnet is 10 cm in diameter, whilst the available 300 K hole, for the vacuum pipe, is only 30.5 mm in diameter, due to the superinsulation necessary as a radiation shield from cryogenic temperature to room temperature. In order to

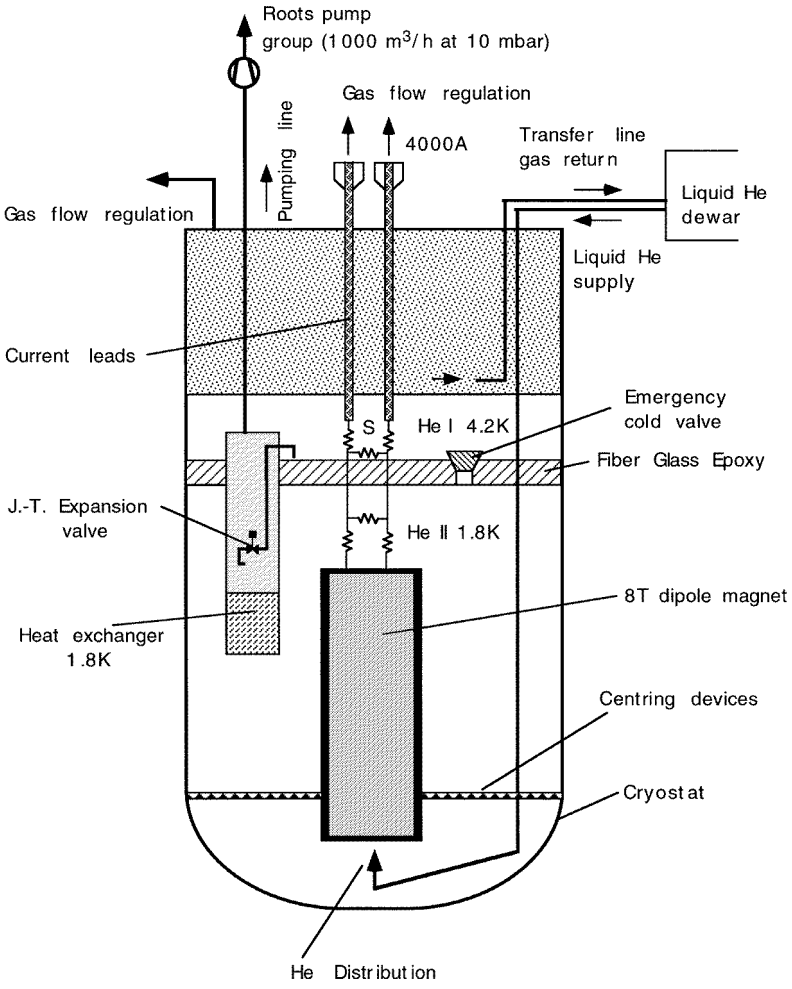

Figure 3. Schematic drawing of the cryostat.

prevent unwanted oscillations of the magnet, special centring devices have been designed and tested to adjust its confinement even at cryogenic temperatures.

The electrical power necessary to the vacuum pumps rotating with the cryostat, is supplied through a multiple ring sliding connector; in the same connector some of the rings are used to transmit the digitized data for the diagnostics as liquid helium levels at different parts of the magnet and cryostat, quench detection system and others.

6. Vacuum requirements

The presence in the magnetic field region of some residual gas will induce on the light beam an ellipticity because of the magnetic birefringence of gases [16] (Cotton–Mouton effect). The Cotton–Mouton effect for several gases has been measured or evaluated theoretically [16]. The value of maximum residual pressure in the vacuum pipe in the magnetic field region depends on the nature of the residual gas itself. To evaluate the required partial

pressure of the components of the residual gas we assume that the gas must not give an effect higher than 10% of the vacuum effect. In table 3 we list the indicative required partial pressure for some of the most common gases following Cotton–Mouton effect values reported in [16].

Table 3. Indicative required partial pressure for some of the most common gases following Cotton–Mouton effect values reported in [16].

Gas	Partial pressure (Torr)
He	2×10^{-6}
H_2	5×10^{-8}
CO	2×10^{-9}
N_2	2×10^{-9}
NO	2×10^{-11}
O_2	2×10^{-10}
CO_2	7×10^{-10}
N_2O	3×10^{-10}
C_6H_6[a]	3×10^{-11}

[a] Other C_xH_y species should have a smaller Cotton–Mouton effect, i.e. a higher required partial pressure.

7. Magnetic shielding

The stray magnetic field of the dipole magnet could induce some systematic effect on the optics and, in particular, on the mirrors of the Fabry–Perot cavity that are also the elements nearest to the magnet. The stray magnetic field on the mirror location has been evaluated by calculation and computer simulation to be around 0.003 T. Some magnetic shielding of the optics will be necessary. The effect of a magnetic field perpendicular to the mirror coating on an interferential mirror has been measured and reported in [17]. As the dominant effect, a Faraday rotation of the light polarization of the order of 3.7×10^{-6} rad T^{-1} per reflection at normal incidence was found. These results depend on the nature and number of the mirror reflective layers and cannot be easily generalized. As far as we know, no measurement of a Cotton–Mouton ellipticity induced on linearly polarized light when reflected by an interferential mirror in the presence of a magnetic field parallel to the reflective surface of the mirror has been published up to now. Indirect effects on the optics may also be generated by a time varying field because of the electromagnetic force proportional to $\partial B/\partial t$ acting on the apparatus. An effect like this has been reported in [9] (note 33).

We will finally design our magnetic shielding after preliminary tests of the effect of the stray magnetic field of our dipole magnet on the optical apparatus.

8. Data acquisition

The basic structure of the data acquisition is designed to write a computer file with the amplitude and the phase of the signal coming from the photodiode PD_T (see figure 2) for some fixed values of the angle θ between the magnetic field and the polarization direction. To define the angular zero we will use a detector sensitive to the stray magnetic field near the rotating cryostat. The absolute angular value will be known via a system that reads the position of some fixed point in rotation with the table supporting the magnet. Using information on θ, and not simply time information, for the data acquisition and processing

should protect us from the frequency instability of the rotating table. The signal from the PD_T photodiode preamplifier is sent to a lock-in amplifier which effectively removes the carrier introduced by the photoelastic modulator. The lock-in internally digitizes the θ analogue output X and Y signals whenever it receives a trigger pulse from the θ angle encoder electronics and sends them to the GPIB interface in the data acquisition computer. The computer stores the data on disk and pauses from time to time to read out the slow controls of the experiment and to display summary information on the ongoing data taking.

9. Experimental set-up

In figure 4 we show a schematic drawing of the final experimental set-up. The horizontal part of the optical apparatus will be placed in a pit on a horizontal granite optical table. A vertical granite optical table will sustain the upper part of the optical apparatus. Both optical tables will be supported by the pavement of the pit. The rotating table with the magnet cryostat will be seated on a concrete beam that will be supported by the floor of the experimental hall. The floor of the pit has been built on poles and should be seismically decoupled from the hall floor. This should somewhat screen the optics from seismic noise coming from the rotation of the magnet cryostat. The whole apparatus should be about 9 m in height, while the distance between the two mirrors of the Fabry–Perot cavity should be around 6 m. The rotating table is able to support several tons of load while rotating at up to 5 Hz.

10. The vacuum optical activity beyond QED

In 1986 Maiani *et al* realized [18] that the existence of a hypothetical neutral light spinless pseudoscalar or scalar particle could also induce a coherent ellipticity on a monochromatic linearly polarized beam traversing a magnetic region.

The total expected ellipticity Ψ_T induced on the light beam will now be the sum of the two contributions

$$\Psi_T = \Psi + \Psi_a \tag{18}$$

where Ψ is given by expression (8) and Ψ_a is due to the particle field, given in [18]:

$$\psi_a = \frac{1}{96}\left(\frac{m_a}{M}\right)^2 L^3 \frac{\lambda}{hc} B_0^2 \tag{19}$$

where m_a is the mass of the hypothetical light particle and M represents the inverse of the strength of its two-photon vertex interaction.

It is important to note that the existence of such a particle would also give rise to an 'apparent rotation' (linear dichroism) ρ of the polarization of the light beam [18]

$$\rho = \frac{1}{16}\left(\frac{B_0}{M}\right)^2 L^2 \frac{h}{2\pi} c. \tag{20}$$

The experimental search for such a particle has so far given negative results [19], with the PVLAS set-up, we will also search for such a dicroism. To be sensitive to the apparent rotation it is sufficient to use, instead of the ellipticity modulator, a rotation modulator as in [9].

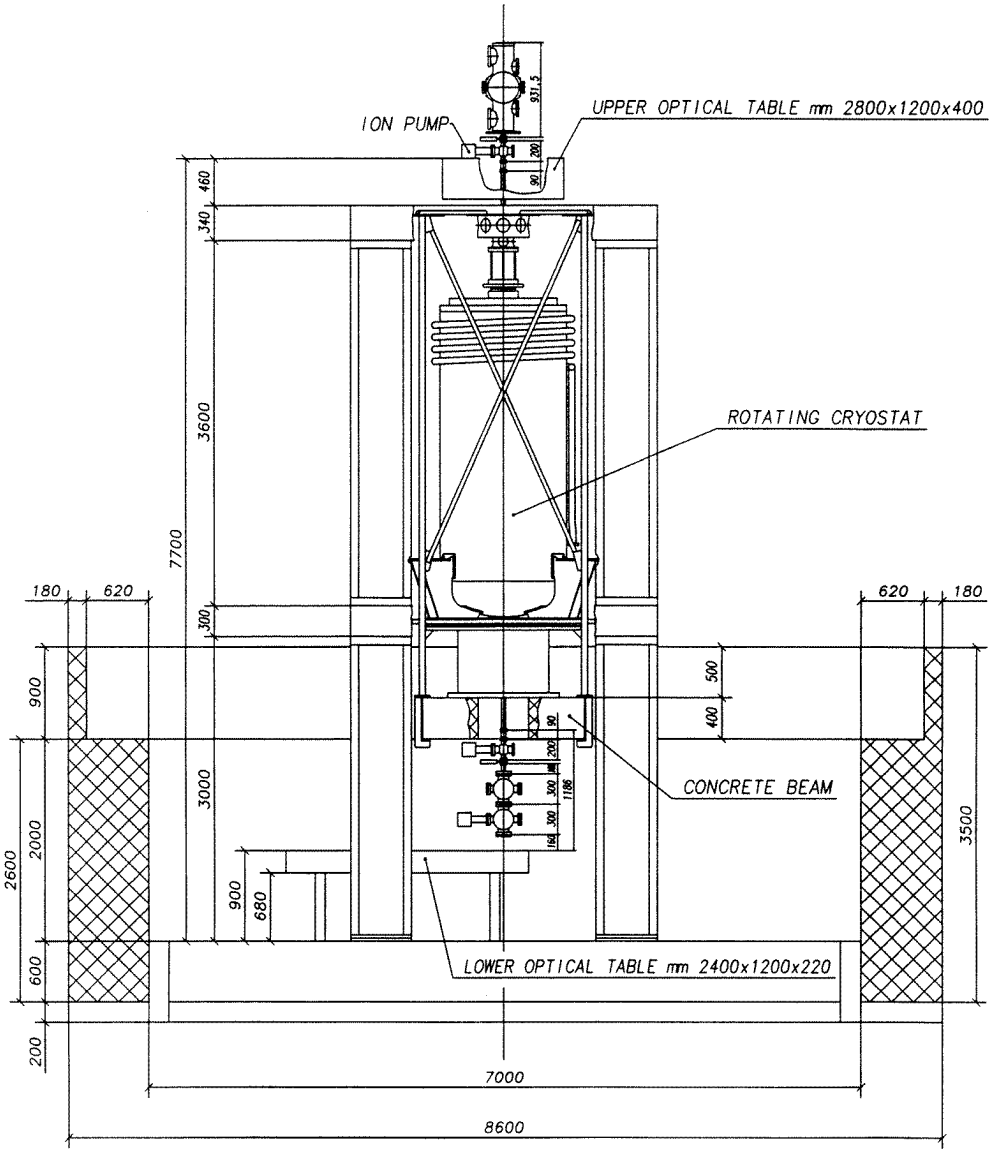

Figure 4. Schematic drawing of the final experimental set-up.

11. Current status and perspectives

The final site of the experiment is at our disposal. The magnet cryostat has been designed and realized, cryogenics tests are currently under way with the magnet in its final location inside the cryostat. In the near future electrical tests will begin.

Tests of the vacuum pumping system are also being conducted; in particular, non-metallic vacuum pipes are under test. Satisfactory results have been obtained using a quartz vacuum pipe. In addition a carbon fibre pipe will be tested.

As for the optical apparatus, we have realized horizontal Fabry–Perot cavities [12] with a very high optical quality factor; we have obtained similar results with vertical Fabry–Perot

cavities. The length of the cavity was 3.2 m and the finesse was about 160 000. We have set up a test vertical ellipsometer based on a smaller 2.1 m cavity of up to 130 000 finesse. For such a cavity we also obtained around 40% transmission. The sensitivity measured was about 10^{-7} rad $\mathrm{Hz}^{-1/2}$, which we believe is mostly limited by the environmental noise of the test area. The situation should improve when the test is conducted in the final experimental area. We have also conducted studies of the intrinsic birefringence of the mirror coatings [11].

During 1998 we should be able to complete the set-up in its final site and start tests of the whole apparatus. The sensitivity should be pushed to 10^{-8} rad $\mathrm{Hz}^{-1/2}$; the cavity finesse should remain around 100 000, while the length should be about 6 m as required; the magnet should provide us with a 8 T field over its 1 m length, the whole cryostat should rotate at about 1 Hz. With these experimental parameters the ellipticity to be measured will be about 5×10^{-11} rad. The signal-to-noise ratio of one should be reached in about 12 h of integration time and a final 20% precision measurement of the vacuum magnetic birefringence could be envisaged.

References

[1] Zavattini E 1996 *Comment. At. Mol. Phys.* **33** 83
[2] Bakalov D *et al* 1994 *Nucl. Phys.* B **35** 180
[3] Iacopini E and Zavattini E 1979 *Phys. Lett.* **85B** 151
[4] Euler H and Heisenberg W 1936 *Z. Phys.* **98** 718
[5] Schwinger J 1951 *Phys. Rev.* **82** 664
[6] Adler S L 1971 *Ann. Phys., NY* **87** 559
[7] Ritus V I 1976 *Sov. Phys.–JETP* **42** 5
Bakalov D 1994 *An Overview of Nonlinear QED Effects for PVLAS* INFN/AE-94/27
[8] Born M and Wolf E 1980 *Principles of Optics* (Oxford: Pergamon)
[9] Cameron R *et al* 1993 *Phys. Rev.* D **47** 3707
[10] Yariv A 1985 *Optical Electronics* 3rd edn (New York: Holt, Rinehart and Winston)
[11] Brandi F *et al* 1997 *Appl. Phys.* B **65** 351
[12] De Riva A *et al* 1996 *Rev. Sci. Instrum.* **67** 2680
[13] Pound R V 1946 *Rev. Sci. Instrum.* **17** 460
Drever R W P, Hall J L, Kowalsky F B, Hough J, Ford G M, Munley A J and Ward H 1983 *Appl. Phys.* B **31** 97
[14] Seyfert P and Claudet G 1988 Superfluidity *Proc. CERN Accelerator School, Superconductivity in Particle Accelerators* 30/5-3/6 239
[15] 1982 *CERN Bulletin* no 28, 12 July
1983 *Mario Morpurgo Group report (PPE)* unpublished
[16] Rizzo C, Rizzo A and Bishop D M 1997 *Int. Rev. Phys. Chem.* **16** 81
[17] Iacopini E, Stefanini G and Zavattini E 1983 *Appl. Phys.* A **32** 63
[18] Maiani L, Petronzio R and Zavattini E 1986 *Phys. Lett.* **175B** 359
[19] Massó E and Toldrà R 1995 *Phys. Rev.* D **52** 1755
Carugno G, Fontana Z, Onofrio R and Rizzo C 1997 *Phys. Rev.* D **55** 6591